Research on Matching Characteristics of Wind Turbine and Generator for Small H-shaped Vertical Axis Wind Turbine

Yong-Chao Xie and Jin-Yan Shi*

Hunan Railway Professional Technology College, ZhuZhou 412001, China
E-mail: shijinyan2008@126.com
**Corresponding Author*

Received 18 May 2021; Accepted 27 May 2021;
Publication 28 July 2021

Abstract

Based on the small H-shaped vertical axis wind wheel model (NACA0016), a CFD wind wheel model was constructed. Based on the principle of moving grid, the grid division of the CFD wind wheel model is completed by using GAMBIT software, and the boundary conditions such as the inlet boundary and the outlet boundary are set reasonably. Then, the turbulence model and the couple algorithm are used to carry out transient simulation calculations, and finally the aerodynamic parameter curves of the two-dimensional CFD wind wheel model are obtained. Based on this, the matching characteristics of the wind turbine and generator of the small H-shaped vertical axis wind turbine are studied. The research results show as follows: when the incoming wind speeds change in range of (2 m/s, 12 m/s), and the power characteristic curve and torque characteristic curve of the generator wind wheel are respectively overlap the best power curve and best torque of the generator, the matching characteristics of the small H-shaped vertical axis wind turbine rotor and generator are optimal, which provides reference for carrying out related research.

Keywords: Matching characteristics, CFD, wind turbine, generator.

Distributed Generation & Alternative Energy Journal, Vol. 36_4, 425–440.
doi: 10.13052/dgaej2156-3306.3645

Wind power generation is widely concerned due to its inexhaustible, non-consuming resources, clean and sanitation, and wide distribution. Manufacturers and research institutions at home and abroad have begun research on small vertical axis wind turbines, they have launched many products with excellent performance. Canadian Cleanfield Energy launched the Darrieus of H-shaped wind turbine with a power of 3.5 KW, low starting wind speed and good wind resistance. The Stato Eolian wind turbine launched by the French company Gual industrie adds a ring of guide blades to the periphery of the vertical axis blades to increase wind speed and rotating torque. The starting wind speed is 2m/s, and it can still be used at 40 m/s. Many domestic manufacturers have also introduced small wind turbines with excellent performance [1–4]. The FDM series vertical axis wind turbine launched by Shanghai MUCE has the advantages of low starting wind speed, strong safety, low noise, and strong wind resistance. Guangzhou Yunpan Wind Energy Technology Co., Ltd. launched a 1KW vertical axis H-shaped wind turbine with a permanent magnet rotor structure, which effectively reduces the resistance torque of the generator. The wind turbine and the generator match well. It is mainly used for municipal streetlight projects in coastal cities. Facilities. Shanghai Linfeng Wind Power Equipment Co., Ltd. adopts the current more popular CFD design method to develop many types of small wind turbines with a power range of 200 W–10 KW and a working wind speed of 4–4.5 m/s. At the same time, with the rapid development of CFD, CFD technology has been widely used in engineering. The application of commercial CFD software has been able to quickly and accurately simulate the unsteady flow field of the H-shaped vertical axis wind turbine, and the characteristics of each blade force and torque can be obtained [5–9].

In this paper, a two-dimensional (2D) model of the wind wheel is established. The unsteady calculations are performed by using the CFD software Fluent. Then, the matching characteristics of wind turbine and generator about small H-shaped vertical axis wind turbine are researched.

1 Model of Theoretical

1.1 Governing Equation

For all flow calculations, it is generally completed by solving the mass equation and momentum conservation equation. When the flow is turbulent,

additional transport equations need to be solved. The pressure-based implicit Couple algorithm is adopted to solve the 2D Reynolds time-averaged N-S equation. The second order upwind difference scheme is used to discretize the convection term, and the moving grid technology is used to perform transient calculations [10–12]. The equation of conservation of mass is shown in Formula 1, and the equation of conservation of momentum is shown in Formula 2.

$$\frac{\partial \rho}{\partial t} + \frac{\partial (\rho u_i)}{\partial x_i} = 0 \tag{1}$$

$$\frac{\partial (\rho u_i)}{\partial t} + \frac{\partial (\rho u_i u_j)}{\partial x_i} = \frac{\partial P}{\partial x_i} + \frac{\partial}{\partial x_i}\left(\mu \frac{\partial u_i}{\partial x_j} + \frac{\partial u_j}{\partial x_i} - \rho \overline{u_i' u_j'}\right) \tag{2}$$

While, the ρ is fluid density. The P is dynamic viscosity of fluid. The $x_i x_j (i, j = 1, 2)$ is coordinate components. The $u_i u_j (i, j = 1, 2)$ is time average velocity component. The $u_i' u_j' (i, j = 1, 2)$ is Pulsating velocity components.

1.2 Turbulence Model

In this paper, the turbulence model adopts the RNG k-ε two-equation model. The RNG model considers the rotation and swirl flow in the average flow. Compared with the standard k-ε model, it can better handle fluids with high strain rates and large streamline curvatures. The external flow field of the vertical axis wind turbine is unsteady, and the rotation of the wind wheel produces strong disturbances. It is more reasonable to choose the RNG k-ε model [13–16]. The transport equation of the RNG model is shown in formula (3) and (4).

$$\frac{\partial (\rho k)}{\partial t} + \frac{\partial (\rho k u_i)}{\partial x_i} = \frac{\partial}{\partial x_j}\left(a_k \mu_{eff} \frac{\partial k}{\partial x_j}\right) + G_k + \rho \varepsilon \tag{3}$$

$$\frac{\partial (\rho \varepsilon)}{\partial t} + \frac{\partial (\rho \varepsilon u_i)}{\partial x_i} = \frac{\partial}{\partial x_j}\left(a_k \mu_{eff} \frac{\partial k}{\partial x_j}\right) + \frac{C_{1\varepsilon}^*}{k} G_k + C_{2\varepsilon} \rho \frac{\varepsilon^2}{k} \tag{4}$$

While, the G_k is $\mu_t \frac{\partial u_i}{\partial x_j}(\frac{\partial u_i}{\partial x_j} + \frac{\partial u_j}{\partial x_i})$, μ_{eff} is $\mu + \mu_t$, μ_t is $\rho C_\mu \frac{k^2}{\varepsilon}$, C_μ is 0.0846, a_k is 1.38, $C_{1\varepsilon}^*$ is $C_{1\varepsilon} - \frac{\eta(1-\eta/\eta_0)}{1+\beta\eta^3}$, $C_{1\varepsilon}$ is 1.42, $C_{2\varepsilon}$ is 1.68, η_0 is 4378, and β is 0.013.

2 Construction of Wind Wheel CFD Model

2.1 Simplified Model of Wind Wheel

Figure 1 is a simplified diagram of the H-shaped vertical axis wind turbine structure. The actual structure of the wind turbine is more complicated, and the main content of this paper is the aerodynamic performance of the wind wheel, so when establishing the geometric model of the flow field, only the wind wheel needs to be considered, so the CFD calculations model need to be simplified. The connecting rods, rotating shafts and other components in the wind wheel affect the flow field around the wind wheel faintly. They can be simplified in CFD modeling. Since the calculation of the flow field outside the wind turbine is transient, it will take a long time if a three-dimensional model is used for calculation. If a two-dimensional model is adopted, it only takes 2 hours to calculate the flow field at each speed with 2 CPUs in parallel, which greatly saves calculation time. The 2D calculation ignores the loss at both ends of the blade, and the calculation result is larger than the three-dimensional calculation, but the calculation result can express the aerodynamic law of wind energy. Analysis reveals that it is better to establish a two-dimensional model for this research. The simplified two-dimensional model is shown as Figure 2. In the Figure 2, r is blade installation radius, α is blade installation angle, and l is blade chord length. The specific parameters of the wind wheel are as follows: Blade airfoil is NACA0016, the number of leaves is 5, the installation angle is 6°, the installation radius is 900 mm, the installation height is 900 mm.

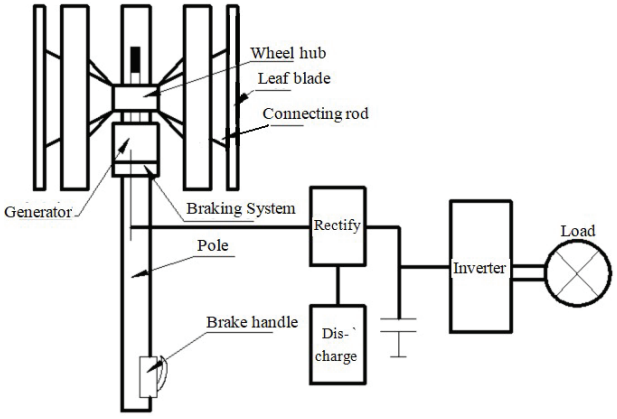

Figure 1 Vertical axis wind turbine structure simplified diagram.

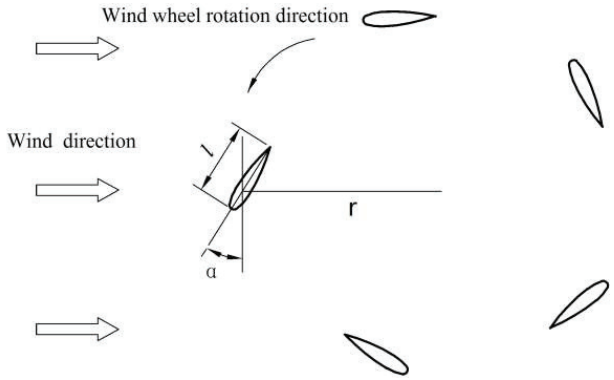

Figure 2 The simplified two-dimensional model.

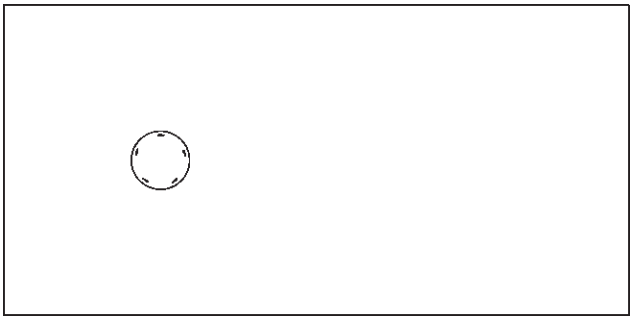

Figure 3 Computational area of the 2D flow field outside the wind turbine.

2.2 Meshing of Wind Wheel Model

Figure 3 shows the computational area of the 2D flow field outside the wind turbine. Using moving grid technology to calculate, the calculation area needs to be divided into a stationary area and a rotating area. The area enclosed by the rectangle and its inner circumference in Figure 3 is the stationary area, and the area inside the circumference is the rotating area [17–19].

When dividing the mesh, divide the two parts separately. The meshing is done in GAMBIT software. The static part has a simple geometric structure and can be divided into blocks with a structured mesh. The geometric structure of the rotating part is complicated. The surrounding blades can be separated into a structured grid with a surface layer, and the inner part of the blade is separated into a structured grid. Figure 4 is a 2D mesh model of the flow field outside wind turbine.

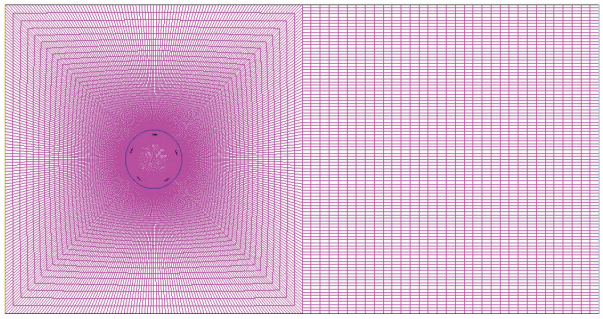

Figure 4 The 2D mesh model of flow field outside wind turbine.

2.3 Setting of Boundary Conditions

The calculation domain of the flow field outside the wind turbine is showed in Figure 4. According to the actual operation of the vertical axis wind turbine, the boundary conditions of the corresponding calculation domain can be determined as follows:

(1) Entrance boundary: The short left side of the rectangle is the speed boundary. The given speed is 2 m/s–12 m/s, and the direction is horizontal.
(2) Outlet boundary: The short right side of the rectangle is the pressure boundary. The given outlet pressure is 0.
(3) Wall boundary: In our research, there are two types of wall boundary. One is virtual wall surface, as the two long sides of the rectangle in Figure 4, the wind speed at the wall is not 0, and it is set as a static sliding wall. The other kind is real wall surface. The blade part is a real wall surface, the blade is rotating, and it is set as a moving wall surface.
(4) Sliding surface: As the mobile grid technology is adopted, the interface between the grid of rotating part and static part should be set to interface [20, 21].

2.4 Calculation Conditions

The transient calculation of the flow field outside the wind wheel is carried out by using the moving grid technology, the RNG turbulence model is adopted, and the pressure-based implicit couple k-ε algorithm is used to solve the problem. The calculation time step is 720 steps, single-step iteration is 60 times, and the wind wheel rotates 2 in each time step. Single-step calculation time $t = \pi\omega/90$, while ω is speed of wind wheel (Rad/s). Given different

speeds respectively, the aerodynamic characteristics of the wind wheel can be obtained through calculation.

2.5 Processing of Calculation Result

The calculation result output by Fluent is the torque coefficient of the blade, which is the curve of the torque changing with the calculation time under a certain working condition. The blades are in different positions at different times, and the torque coefficient also changes with time. For the sake of making the calculation results comparable, take the average of the two cycles as the final calculation result, and multiply the torque coefficient by a coefficient of 0.6125 to obtain the wind wheel torque. From the wind wheel torque and the wind wheel speed, the wind energy utilization rate and tip speed ratio of the wind wheel can be calculated. Change the speed and recalculate to get the wind wheel performance curve.

The wind energy utilization rate refers to the amount of energy that a wind turbine absorbs from natural wind energy, as shown in formula 5.

$$C_p = \frac{2M\omega}{\rho S v^3} \tag{5}$$

In this formula, M is fan torque, ρ is air density, ω is fan speed, S is sweeping area, and v is air velocity.

The tip speed ratio represents the speed of the wind turbine, which is expressed by the ratio of the blade tip circumferential velocity to wind speed λ, as shown in formula 6.

$$\lambda = \frac{2\pi nr}{v} \tag{6}$$

In this formula, n is wind speed, r is installation radius.

3 Analysis of Simulation Result

Under different incoming wind speeds, the wind energy utilization rate, torque and power of the wind wheel vary greatly. The wind wheel has an optimal running speed at different incoming wind speeds, and the efficiency is the highest at this time. For the sake of maximizing the conversion of the mechanical energy obtained by the wind wheel into kinetic energy, the characteristics of the wind wheel must be matched with the characteristics of the generator, so as to realize the wind energy maximum utilization and improve the operating efficiency of the wind generator. This article mainly discusses

the power and torque characteristics of the generator. When the incoming wind speeds change in range of (2 m/s, 12 m/s), the power and torque curves of the wind wheel are calculated to study the matching characteristics about the wind wheel and generator.

3.1 Research and Analysis of Wind Wheel Aerodynamic Performance

Figure 5 is the curve of wind energy utilization rate of the wind wheel with the tip speed ratio under different incoming wind speeds. The tip speed ratio corresponding to the different speeds of the wind wheel can be calculated by Equation (6). Figure 5 shows that wind speed affect the efficiency of wind turbine utilization significantly. When the tip speed ratio is below 1.5, the wind energy utilization curve at each wind speed basically overlaps, and the wind energy utilization rate of the wind turbine at each wind speed has a small difference. When the tip speed ratio is above 1.5, the difference in wind energy rate at each wind speed is obvious. When the wind speed is from 2 m/s to 12 m/s, the higher the speed, the higher the maximum wind energy utilization rate. At every incoming wind speed, the wind energy utilization rate increases first and then decreases with the peak speed ratio of wind energy. The tip speed ratio is about 2.0, and the wind energy utilization rate reaches the maximum value.

From Figure 6, we can obtain the variation of the wind wheel torque with the rotation speed under different incoming wind speeds. We can gain that under different incoming wind speeds, the rotating speed range of the

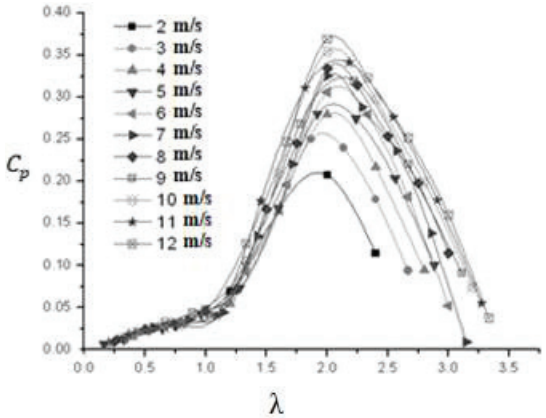

Figure 5 Wind energy utilization rate under different incoming wind speeds.

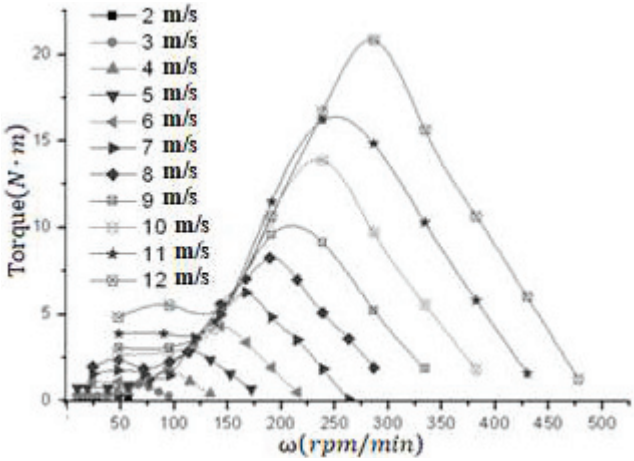

Figure 6 Under different incoming wind speeds, the wind wheel torque varies with the speed.

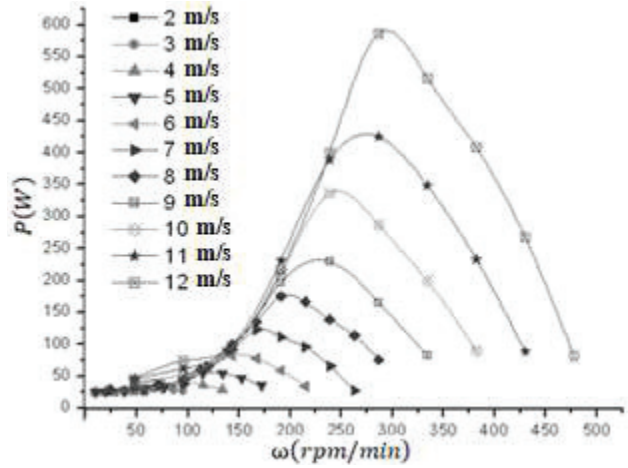

Figure 7 Under different incoming wind speeds, the wind wheel power varies with the speed.

wind wheel is also quite different. When the wind speed is 2 m/s, the wind wheel torque is almost zero during the working process. If the wind speed is above 3 m/s, the wind wheel torque gradually increases, and if the wind speed reaches 12 m/s, the torque of the wind wheel reaches the maximum value.

Figure 7 is a graph showing the change of wind wheel power with rotation speed under different wind speed and incoming wind speed. The change

of power with speed at different wind speeds is basically the same as the change of torque with speed. At low speeds, the wind wheel power is lower at different wind speeds, and the power curves almost overlap. When the working speed increases, the power of the wind wheel increases significantly.

From Figures 6 and 7 that at different wind speed, it corresponds to the maximum torque and power of wind wheel respectively. During the running of the wind turbine, the rotation speed of generator is always equal to the wind wheel rotation speed. If the generator rotation speed is always equal to the wind wheel speed under different incoming wind speeds, the generator will maximize the conversion of wind energy into electrical energy.

3.2 Optimal Power Matching Between Wind Wheel and Generator

Under different incoming wind speeds, if the optimal operating points of the wind wheel power curve and the optimal operating points of the torque curve are connected, the optimal output power curve of the wind wheel is obtained. And if the optimal operating points of the wind wheel torque curve are connected, the optimal output torque curve of the wind wheel is obtained. As long as the power and torque curves of the generator coincide with the optimal power and torque curves of the wind wheel, the wind turbine system composed of the generator and the wind wheel acquires the optimal matching characteristics.

Figure 8 is the best torque curve of the wind wheel. And Figure 9 is the best power curve of the wind wheel. When the selected motor torque curve and power curve coincide with the best torque and best power curve respectively, the obtained wind energy can be utilized to the maximum extent.

Figure 10 shows the matching curves of the output power between wind wheel and the generator under different incoming wind speeds. Curves a, b, and c are the power curves of the generator under different loads. The intersection between the power curve of the generator and the wind wheel is the operating point of the wind generator. The intersection points of the three load curves and the wind wheel power curve are different, and the corresponding power and speed are also different.

The output power of load curve c and load curve a is basically the same, but the speed of the wind wheel corresponding to curve a is obviously lower than that of curve c. When the rotating speed is too high, the stability and reliability of the wind turbine system will be significantly reduced. Therefore, the load size of the generator can be changed while the output power remains

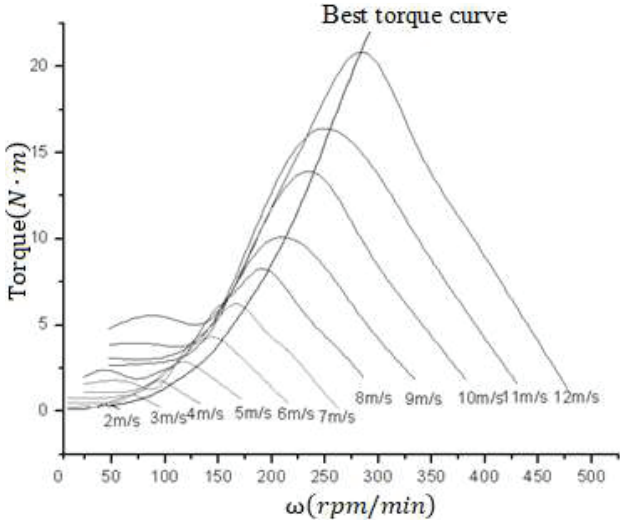

Figure 8 Best torque matching diagram.

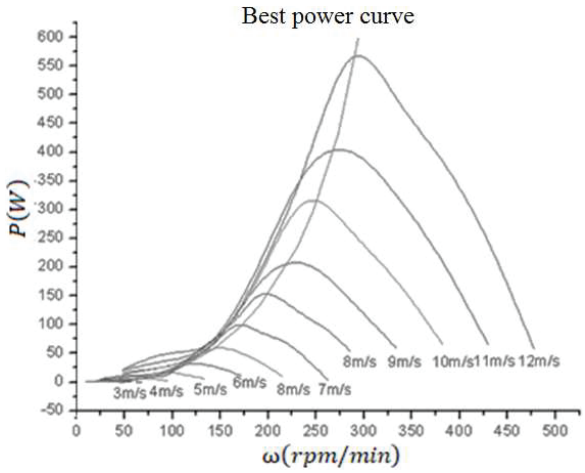

Figure 9 Best power matching diagram.

unchanged, thereby reducing the speed of the wind wheel. When the load power curve is a and c, the load size of the generator can also be adjusted and changed to make the wind generator work at the optimal speed to ensure the maximum output power.

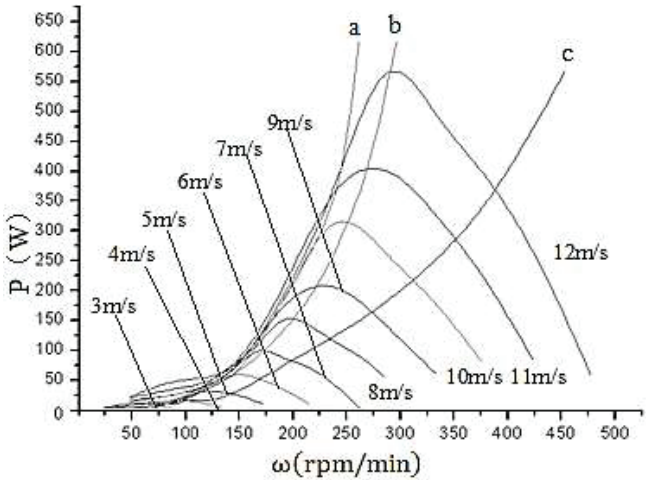

Figure 10 Matching curves of wind turbine and generator under different loads.

4 Conclusions

(1) Under different incoming wind speeds, wind energy utilization rate changes with the tip speed ratio: if the tip speed ratio is above 1.5, the difference in wind energy rate at each wind speed is obvious. When the wind speed changes from 2 m/s to 12 m/s, the higher the wind speed, the higher the maximum wind energy utilization rate. At every incoming wind speed, the wind turbine's wind energy interest rate increases first and then decreases with the peak speed ration of wind energy. The peek speed ratio is about 2.0, and the wind energy utilization rate reaches the maximum value.

(2) Under different incoming wind speeds, the torque of the wind wheel changes with the speed: if the speed of wind is greater than 3 m/s, the wind wheel torque gradually increases, and if the wind speed reaches 12 m/s, the wind wheel torque reaches the maximum value.

(3) At different incoming wind speeds, the power of the wind wheel changes with speed: when the speed is very low, the power of the wind wheel is low, and the power curves almost overlap. When the working speed of the wind wheel increases, the power of the wind wheel increases significantly.

(4) Figures 8 and 9 are the best torque and power curves of the wind wheel respectively. When the selected motor torque and curve and power curve

coincide with the best torque and best power curve respectively, wind energy can be used to the maximum extent.

(5) Under different incoming wind speeds, the output power of the wind wheel matches the generator: the intersection points of the three load curves and the wind wheel power curves are different, and the corresponding power and speed are not the same. By adjusting the load, the wind generator can be The output power and working speed are adjusted.

Acknowledgment

This work was supported by Hunan Provincial Natural Science Foundation of China (NO:2020JJ6095).

References

[1] Fei Rong, Xiaoyue Xu, Shijia Zhou et al. Optimized strategy for DFIG wind farm considering turbine fatigue[J] International Journal of Electrical Power and Energy Systems, 2020.

[2] Wu Yun-ke, Li Zhi-qiang, Zhang Zhi-hong, Liu Li-fang. Numerical Study on the Aerodynamics Design for MW-Level H-shaped Vertical Axis Wind Turbine[J]. Journal of Engineering for Thermal Energy and Power, 2019(6).

[3] Jin Xin, Ju Wenbin, Ren Haijun, Yang Xiangang. Research of Aerodynamic Analysis Method and Operation Law of H-Shaped Vertical Axis Wind Turbine[J]. Acta Energiae Solaris Sinica, 2017(10).

[4] Liu, Ran Hui. The Analysis of Power Performance for Small H-Vertical Axis Wind Turbine, Advanced Materials Research, 2013.

[5] Xing Zhi, Duan Xiangjun, Liu Lei. MPPT for wind power system with switched reluctance generator, 2018 13th IEEE Conference on Industrial Electronics and Applications (ICIEA), 2018.

[6] Shi Jinyan, Xie Yongchao. Analysis of Performance of Small Vertical Axis Wind Power Generator with NACA0016 Airfoil[J]. Science Mosaic, 2015(8).

[7] Xiaojing Sun, Wanli Zhou, Diangui Huang, Guoqing Wu. Preliminary study on the matching characteristics between wind wheel and pump in a wind-powered water pumping system[J]. Journal of Renewable and Sustainable Energy, 2011.

[8] M. Zheng, X. Zhang, L. Zhang, H. Teng, J. Hu, M. Hu. Uniform Test Method Optimum Design for Drag-Type Modifified Savonius VAWTs by CFD Numerical Simulation[J]. Arabian Journal for Science and Engineering, 2017.
[9] Lin Pan, Haodong Xiao, Yanwei Zhang, Zhaoyang Shi. Research on Aerodynamic Performance of J-type Blade Vertical Axis Wind Turbine, 2020 Chinese Control And Decision Conference (CCDC), 2020.
[10] M. Ghasemian, Z.N. Ashrafi, A. Sedaghat. A review on computational fluid dynamic simulation techniques for Darrieus vertical axis wind turbines[J]. Energy Conversion & Management, 2017(1).
[11] Bi Jihong, Wu Ji, Guan Jian, Wang Jian. Influence of Wind Speed, Stay Cable Inclination Angle and Wind Yaw Angle on Formation of Rivulets[J]. Transactions of Tianjin University, 2016(6).
[12] Wu Chutian, Yang Xiaolei, Zhu Yaxin. On the design of potential turbine positions for physics-informed optimization of wind farm layout[J]. Renewable Energy, 2021.
[13] Kou Peng, Wang Chen, Liang Deliang et al. Deep learning approach for wind speed forecasts at turbine locations in a wind farm[J]. IET Renewable Power Generation, 2020.
[14] Han Zhimin, Li Shenggang, Liu Heng. Composite learning sliding mode synchronization of chaotic fractional-order neural networks[J]. Journal of Advanced Research, 2020.
[15] Bastankhah Majid, Welch Bridget L., MartínezTossas Luis A. et al. Analytical solution for the cumulative wake of wind turbines in wind farms[J]. Journal of Fluid Mechanics, 2021.
[16] Ben Hoen, Jeremy Firestone, Joseph Rand et al. Attitudes of U.S. Wind Turbine Neighbors: Analysis of a Nationwide Survey[J]. Energy Policy, 2019.
[17] Sung-ho Hur. Modelling and control of a wind turbine and farm[J]. Energy, 2018.
[18] D.H. Wood, V.L. Okulov, D. Bhattacharjee. Direct calculation of wind turbine tip loss[J]. Renewable Energy, 2016.
[19] Li Yanting, Wu Zhenyu. A condition monitoring approach of multi-turbine based on VAR model at farm level[J]. Renewable Energy, 2020, 166.

[20] Shaler Kelsey, Jonkman Jason Fast. Farm development and validation of structural load prediction against large eddy simulations[J]. Wind Energy, 2020.
[21] Lu Kai Hung, Hong Chih Ming, Xu Qiangqiang. Recurrent wavelet-based Elman neural network with modified gravitational search algorithm control for integrated offshore wind and wave power generation systems[J]. Energy, 2019.

Biographies

Yong-Chao Xie received his B.Sc. degrees in Communication Engineering from Lanzhou Jiaotong University, China; M.Sc. degree in Communication and Information System from Southwest Jiaotong University, China; Now, Yong-Chao Xie is an associate professor at Hunan Railway Professional Technical College, and he is a key young teacher in Hunan Province, China; His research field of centers on motor control technology.

Jin-Yan Shi received her B.Sc. degrees in Machine Design and Automation from Lanzhou Jiaotong University, China; M.Sc. degree in Drive Technology and Intelligent System from Southwest Jiaotong University, China; Now, Jin-Yan Shi is an associate professor at Hunan Railway Professional Technical College, and she is a key young teacher in Hunan Province, China; Her research field of centers on CFD modeling and simulation.